J Vis (2017) 20:277–288
DOI 10.1007/s12650-016-0399-x

REGULAR PAPER

S. Peralta · F. Aragón · A. Torres · E. Serrano · I. Carvajal · A. Medina

Visualization of steam injection into homogeneous porous media

Received: 9 November 2015 / Revised: 26 August 2016 / Accepted: 20 September 2016 / Published online: 13 October 2016

Abstract In this study we describe the important features of the process of steam injection through non-consolidated porous media made of sand. We have analyzed the resulting fluid flow patterns through normal and infrared visualization by varying the injection pressure into a horizontal cylindrical pipe and a circular cell on a vertical position. Such configurations mimic those occurring under the steam assisted gravity drainage (SAGD) in tertiary recovery from oilfields and geothermal reservoirs. We describe some characteristics of the ubiquitous condensation front in both experimental arrays. In the first case, a glass pipe filled with sand was subjected to steam injection at different pressures. In the second case, a circular cell on a vertical position brimful of sand cell was subjected to similar processes. For each case, the existence of several types of condensation fronts, depending on the injection pressure, has been evidenced by means of digital and infrared visualization which gives mutually complementary information.

Keywords Flow Trough Porous Media · Flow visualization and imaging · Experimental aspects

1 Introduction

Geothermal systems are located in the upper part of the earth's crust for about 10 km and consist of permeable rock with temperatures up to 573–673 K and pressures from 1013 to 4060 kPa (Grant et al. 1982). These systems are typically saturated with steam and liquid and present plenty of different fluid flow phenomena. There is a considerable interest in the knowledge of thermal and spatial evolution of steam and

S. Peralta (✉) · E. Serrano
Instituto Mexicano del Petróleo., Eje Central Lázaro Cárdenas 152, Col. Atepehuacán, Gustavo A. Madero, Distrito Federal, 07730 México, DF, Mexico
E-mail: peraltasalomon@hotmail.com

F. Aragón · I. Carvajal
Instituto Politécnico Nacional, ESIME Zacatenco, Av. Unidad Profesional Adolfo López Mateos, Col. Lindavista, Del. Gustavo A. Madero, México, DF 07738, Mexico
E-mail: micme2003@yahoo.com

I. Carvajal
E-mail: icarvajal@yahoo.com

A. Torres · A. Medina
ESIME Azcapotzalco, Instituto Politécnico Nacional, Av. de las Granjas No. 682, Col. Santa Catarina, Delegación Azcapotzalco, México, DF 02250, Mexico
E-mail: higherintellect@hotmail.com

A. Medina
E-mail: amedinao@ipn.mx

its condensate within the geothermal systems. These phenomena have some features in common with water and steam injection into the oil reservoirs (Yortsos 1984).

All of these systems can be properly studied at laboratory scale by means of a representative number of variables which can be combined to obtain dimensional groups (Geertsma et al. 1956).

The main purpose of this study is to describe the motion of steam and its fluid condensate within a non-consolidated porous medium, taking into account the forced convective heat transfer associated with fluid injection. To reach our goals in the next Section, we describe the main experimental configurations here studied. Then in Sect. 3.1 the initial experiment, characterized by an infrared image of a free steam jet emerging to the atmosphere is presented. Such case will be interesting for the study of the displacement of the condensate front during the steam injection in a porous medium of tubular geometry at different pressures and temperatures. To our knowledge, the use of infrared thermograpy has scarcely been employed to characterize two-phase flows in porous media (Astarita and Carlomagno 2013). Nevertheless, this non invasive technique gives noteworthy clues for heat transport.

The temperature and injection pressure affect the displacement pattern of the condensation front within the unconsolidated porous medium. During the steam injection, the temperature across the cell changes and the mobility ($M = k\backslash\mu$), which is defined as the ratio of rock permeability k to apparent fluid viscosity μ (Speight 2016) is enhanced (Yun 2008), since the viscosity decreases and consequently, the mobility rises. In Sect. 3.2 the first geometry considered was a horizontal cylinder, filled with dry Ottawa sand, in which steam is injected at different pressures, to visualize the formation of the condensation front that goes from a nose-like to a piston-like shape. In Sect. 4, we studied the movement of a condensate front during the steam injection into a radial porous cell where the effect of the gravity becomes significant. Using both geometries it is evident that when the steam is injected a complex condensation front is formed. It is strongly related to the value of the injection pressure and the gravity. Finally in Sect. 5, the conclusions of this work are given.

2 Experiments

2.1 Experimental setup

Three different experiments were conducted to visualize the steam and condensate front behavior in three different configurations, they are described as the emerging jet, the horizontal porous cell and the porous radial cell.

For the emerging jet configuration (Fig. 1), steam is suddenly discharged through an empty tempered glass tube 0.42 m length, 0.039 m internal diameter and 0.003 m wall thickness. For all the experiments the steam was injected by means of a hose of 0.0127 m connected at the centre of the inlet screwed cap. The steam emerges to the atmosphere from an horizontal nozzle which was made with an array of five holes 0.003 m radius that were drilled in a DURAN GL45 screw cap which was screwed at the rear end of the tube. A frontal view of the nozzle can be seen in the inset of Fig. 1a. In this experiment, the saturated steam was delivered by a steam generator at a pressure of 98.1 kPa. For the steam injection through a horizontal porous cell, we used a non-consolidated porous medium made of Ottawa silica sand (20–30 mesh) under ASTM C778 standard. We assume approximate values reported elsewhere, thus the porosity ϕ of 0.5 and a permeability of $k = 2.0\ \mathrm{E} - 7\ \mathrm{m}^2$ (Nield and Bejan 2006). The silica sand was poured into the tube and manually compacted by means of vibration. Under this specific configuration, experiments at three different injection pressures are reported to visualize the steam injection process. A cap with orifices was also screwed at the rear end of the tube, which allowed the fluid to flow but not the sand to go out. Therefore, the steam injection in the tube obeys a pressure gradient between the injection and the atmospheric pressure. A scheme of this array can be observed in Fig. 2.

Finally, for the porous radial cell, steam was injected into a radial configuration, vertically oriented as to observe the behavior of the injection process in a similar array as that of Butler (1991). In this case, the porous matrix was contained by placing two circular plates of tempered glass 0.0127 m thick in a parallel array, conforming a radial cell with a diameter $\phi_{glass} = 0.40$ m and a thickness of the sand layer $e_{sand} = 0.056$ m. The steam injection port was located 0.086 m far from the bottom of the cell. The cell perimeter was hermetically sealed to avoid the exit of fluids. At the upper part of the cell there was an exhaust hole since steam pushes the air to the outside. The experimental scheme can be observed in Fig. 7.

All experiments were recorded with two different cameras. For the infrared measurements, a digital FLIR camera (ThermaCAM SC660) with a maximum resolution of 640 × 480 pixels and a spatial

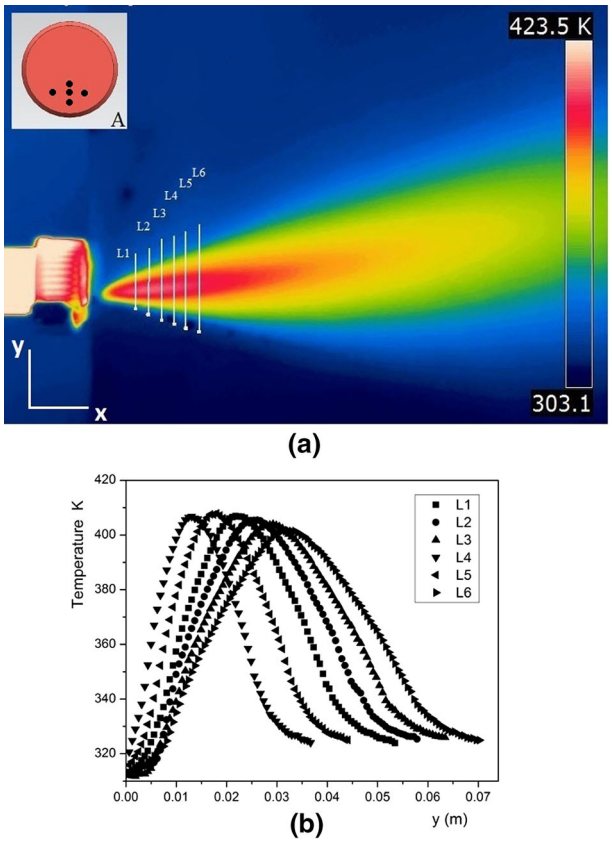

Fig. 1 **a** Infrared image of a steam jet emerging to the atmosphere. In *inset A* we depict a scheme of the nozzle with its injection orifices (*black dots*). **b** Plot of the temperature distribution as a function of the vertical distance along the *y-axis*. The plotted data were obtained from the steam jet along the lines L1 to L6

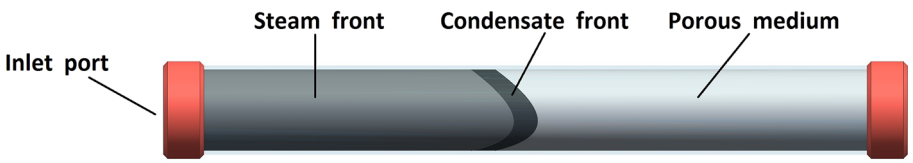

Fig. 2 General scheme of the horizontal porous cell. The direction of the flow is observed to be on the (x) axis

sensitivity (ie., a measure of the size of the details which can be resolved (McHugh 1991) of 0.65 mrad. This camera has a measuring range of 233.15–1773.15 K, with a thermal sensitivity of 30×10^{-3} K and a measurement error of 1.0 %. It is able to reach infrared sequences every 10 s. To record the advance of the condensates, a conventional reflex camera Nikkon D5100 with a resolution of 16.1 megapixel. Both cameras were placed pointing towards the center of the test section at approximately 1 m distance. All the set of experiments were carried out at room temperature ($T_\infty = 299$ K) and at atmospheric pressure.

3 Steam injection into an horizontal tubular matrix

3.1 Jet

For this experiment and to show the advantages of the infrared thermography technique (IRT), in Fig. 1a we started by showing an infrared image of a turbulent steam jet emerging to the atmosphere from an horizontal

nozzle. In this experiment, steam is discharged and travels within an empty tempered glass tube. Instantaneously, the steam reaches the rear end of the tube and is discharged to the atmosphere as a jet by the nozzle. A drawing of the frontal face of the nozzle is shown at the left upper corner of Fig. 1a inset **A**. With the aid of the camera software in Fig. 1b the temperature distribution along six equally spaced vertical lines (L1 to L6) is plotted as a function of the vertical distance (y).

3.2 Horizontal porous cell

This second set of experiments were intended to show how steam and the condensates front migrate within a dry non-consolidated porous medium. It is important to be aware that close to the side walls, the porosity of the porous medium is slightly higher respect to the porosity in the core (Bejan 2013), Chen (1996). As a consequence of this condition, the mechanical contact among the grains within the container is enhanced and the thermal contact is improved. The general scheme of the experiment can be seen in Fig. 2.

During the injection processes, saturated steam passes trough the host porous medium which is initially at room temperature ($T_\infty = 299$ K), due to the imminent heat exchange, part of the steam condenses and moves as a condensate front (Woods 2012). This condensate front, as reported in literature, may adopt several shapes that go from a nose at low pressures to a fully developed piston-like flow Dudfield and Woods (2012). These patterns of condensate fronts will be discussed later on.

The characterization of the condensate front velocity inside the porous matrix is essential to understand the role of pressures and temperatures in its shape.

In this manner, the condensate front was visualized moving through the porous medium at three different initial injection pressures: $P_i = 24.5$, 49.1 and 98.0 kPa. The main parameters of this set of experiments are shown in Table 1.

The Froude number Fr, that represents the ratio of inertial forces to the gravity forces, will help us to characterize the shape of the condensation front during the steam injection. For a porous medium, the (dimensionless) Froude number can be introduced as follows:

$$Fr = \frac{Q^2}{\phi^2 A^2 g D}, \tag{1}$$

where Q is the flow rate in m^3/s, A is the cross sectional area of the pipe in m^2, g is the gravity acceleration in m/s^2, D is the internal diameter of the tube in m and ϕ is the porosity.

For the first experiment, the magnitude of the Froude number is $Fr = 0.0056 << 1$, which gives a sub-critical fluid flow i.e., for such conditions the gravity forces dominate over the inertial forces during the phenomenon, hence the advancing of the condensate front adopts a shape that can be seen in Fig. 3a. We note that gravity has an important role at Fr values because the shape of the condensate has a small protuberance at its lower part, which is maintained along the flow of the entire pipe, resulting in a nose flow (Dudfield and Woods 2012).

In the second experiment, the Froude number $Fr = 0.019 < 1$, so the shape of the condensate front is flatter with respect to the first case, as shown in Fig. 3b, resulting also in a sub-critical flow.

For the last experiment, the Froude number was $Fr = 0.3 < 1$, which once again corresponds to a sub-critical flow. But in this case, it is shown that the condensate front reaches the piston-like flat flow. The shape of the condensate front is shown in Fig. 3c.

The corresponding displacement of the condensate front was plotted, as a function of time and is presented in Fig. 4. Notice that for high pressures the front advances almost nearly, as a function of time, but for lower pressures the motion of the front deviates.

The last part of this experimental section is devoted to visualize the temperature distribution on the tube surface during the steam injection with the aid of the infrared camera. It is comment worthy that the effective thermal conductivity is enhanced by two new factors, the increasing internal pressure (Yun and

Table 1 General parameters used in the experiments

Experiment	Injection pressure (kPa)	Flow rate (m^3/s)	Froude number (Fr)
1	24.5	$Q = 0.0000278$	$Fr = 0.0056$
2	49.1	$Q = 0.0000516$	$Fr = 0.019$
3	98.0	$Q = 0.0001030$	$Fr = 0.3$

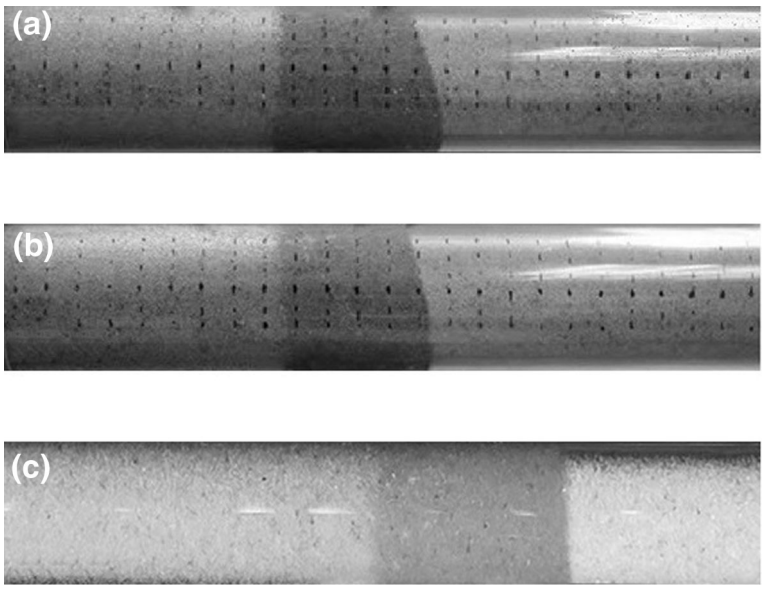

Fig. 3 Snapshots showing the condensation front at three different injection pressures. In A at P_i = 24.5 kpa, in B at P_i = 49.1 kPa and in C at P_i = 98.0 kPa

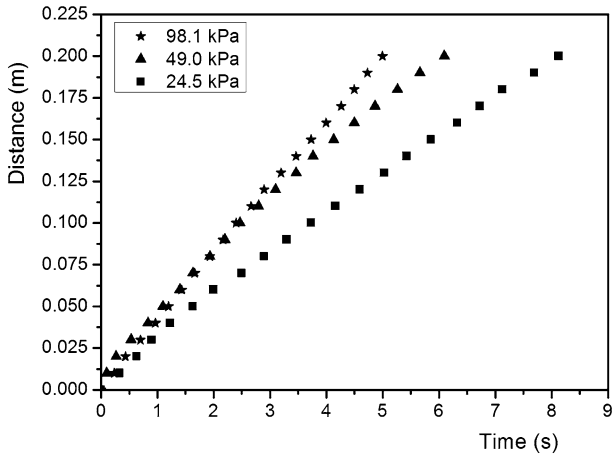

Fig. 4 Plots of the displacement of the steam front as a function of time, for the three different values of the initial injection pressure (P_i)

Santamarina 2008) and the condensate. A representative thermography sequence is shown in Fig. 5 to visualize the temperature behavior. This sequence corresponds to the case of an initial injection pressure $P_i = 24.5$ kPa. The surface temperature measured by the IR Camera is approximately the actual temperature in the porous medium, close to the wall, but with a delay due to the wall thickness of the glass tube, which imposes a diffusive process of heat transfer from the inner tube wall to the outer wall, and therefore, there is a diffusion time that is defined as follows $t_d = \delta^2/\alpha$ where $\delta = 0.006$ m is the side wall thickness of the glass wall and $\alpha = 6.6 \times 10^{-7}$ m^2/s is the thermal diffusivity of the glass, in this way the delay time is approximately of t_d = 54.54 s.

The maximum speed reached on the other by the condensate water front by comparing only experiments 1 and 2 was 0.1 m/s. On the other hand in experiment 2, the minimum velocity of the condensate front presents values of less than 0.04 m/s. A comparative plot of the velocity of the fronts (obtained from the data of Fig. 3) at an initial pressure P_i of 24.5 and 49.0 kPa respectively, is shown in Fig. 6.

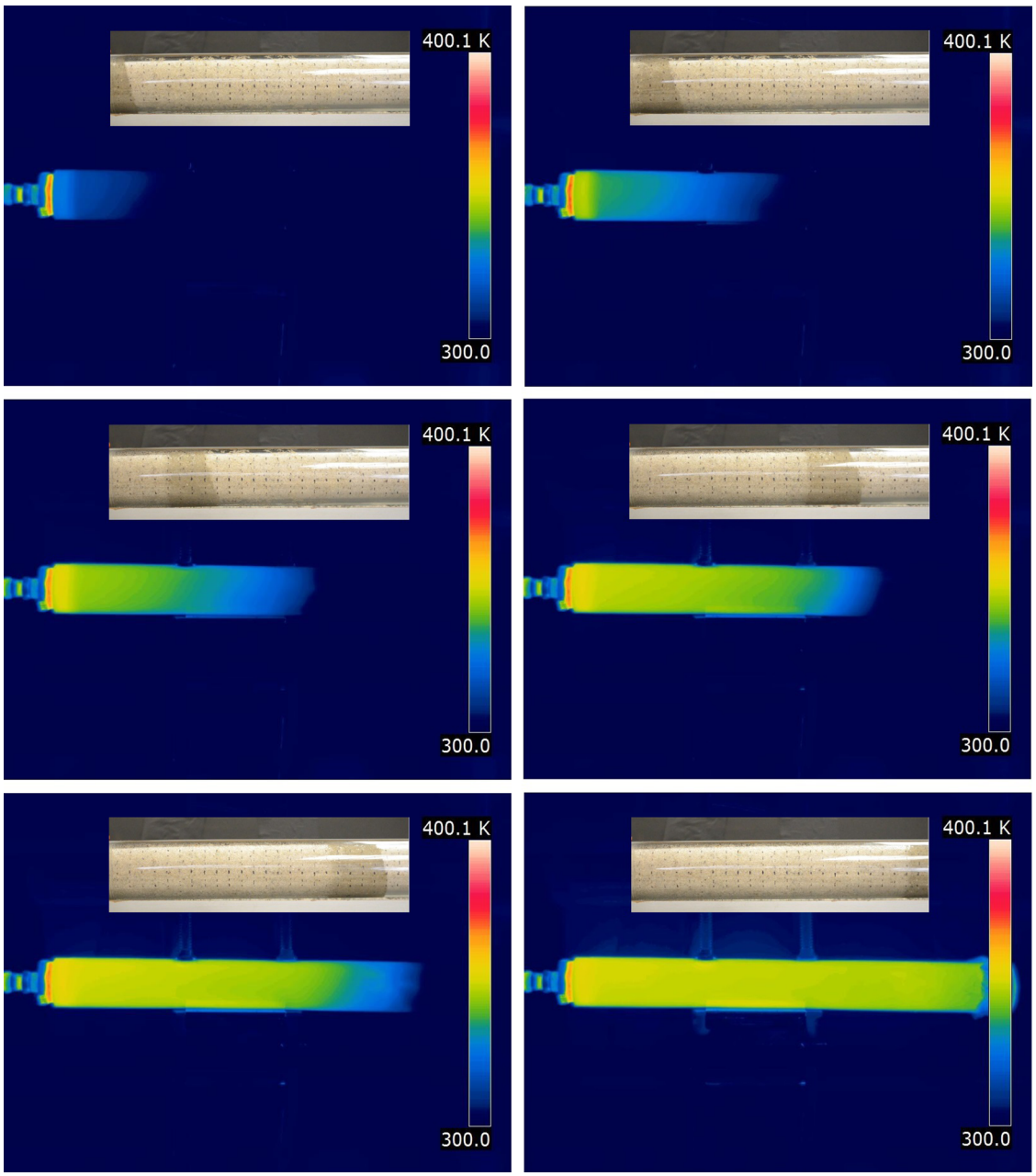

Fig. 5 Infrared snapshots of the condensate flow at an injection pressure ($P_i = 24.5$ kPa). The inset placed at the top of each snapshot shows the respective visual images of the condensate fronts at the same time

In the estimation of velocities, these could be theoretically estimated accurately by means of Darcy's equation, introduced by Nield and Bejan (2013). As it can be seen in Eq. (2).

$$v = -\frac{k}{\mu}\frac{\Delta P}{L}. \tag{2}$$

This last equation can be expressed as:

$$x = -\frac{k}{\mu}\frac{\Delta P\, t}{L}. \tag{3}$$

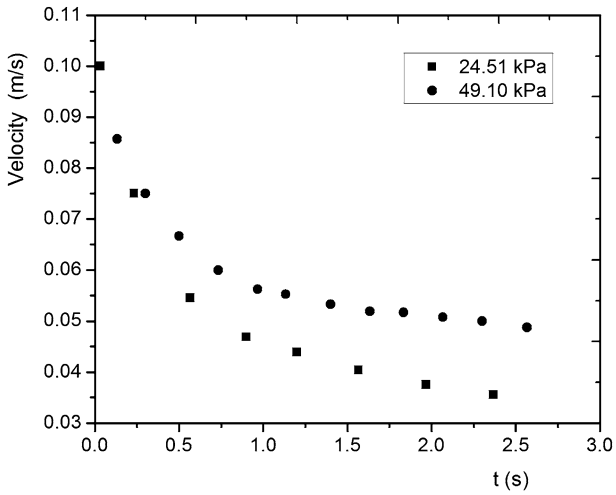

Fig. 6 Plot of velocity of the condensate front as a function of time at two different initial injection pressures of $P_i = 24.5$ kPa and $P_i = 49.0$ kPa

The linear behavior of x vs. t in Eq. 3 was expected, but as it can be clearly seen in Fig. 6 the speed of the condensate front is not constant. Notice that perhaps Capillary effects plays an important role due to the presence of the condensate front, or the changes in the viscosity of the steam when it interchanges heat with the host medium resulting in a nonlinear movement of the condensate front due to the viscosity μ is a function of the temperature.

4 Steam injection into a porous circular vertical cell

In this series of experiments, we injected saturated steam at different pressures into a radial configuration, vertically oriented, to observe the behavior of the condensate front. We found that for this case the condensate front grows radially from the injection port until the boundaries of the cell are reached.

The asymmetric location of the injection hole mimics, for instance, the pipes array used in tertiary oil recovery method known as steam assisted gravity drainage (SAGD). In such process, the steam injection piping crosses horizontally the reservoir and produces radial steam within it (Butler 1991). In this particular array, gravity plays an important role, specially if the oil viscosity is low and the porous medium has a high permeability (Shreve et al. 1956). The scheme of the experiment is shown in Fig. 7. In this case, the diffusion time across the sidewalls was $t_d = 244.37$ s because the thickness of sidewalls is $\delta = 0.0127$ m. For these series of experiments the temperature and pressure of the steam were kept constant.

The Froude number Fr was introduced in Sect. 3.2 and we slightly modified it for the circular porous cell array, this time by replacing D with the diameter of the porous vertical circular cell.

To observe the shape of the condensate front inside the radial porous cell, experiments with three different injection pressures, $P_i = 49.1$, 245.1 and 14.7 kPa, were carried out. The main parameters of this set of experiments are shown in Table 2.

In the first experiment, steam was injected into the porous radial matrix at an initial pressure of $P_i = 49.1$ kPa. We found that the saturated matrix reached a maximum temperature of $T = 357.45$ K, which was measured with the Infrared camera. The condensate was displaced radially due to the magnitude of the injection pressure into the homogeneous matrix, a sequence of the radial advance or the condensate front can be seen in Fig. 8.

Plots, obtained from experiments of steam injection into the porous cell of silica sand, are given in Fig. 9. Steam was injected at an initial pressure of $P_i = 49.1$ kPa. In Fig. 9a we show the radial displacements of condensed water in the cell. Meanwhile in Fig. 9b we can observe the temperature evolution at different instants of time.

In the sequence of thermal images of Fig. 10, a radial temperature distribution can be observed. In addition, this temperature field evolves with time, the first image shows the radial system instants after the steam injection begins, as the steam injection continues, we observe in subsequent images a change in the

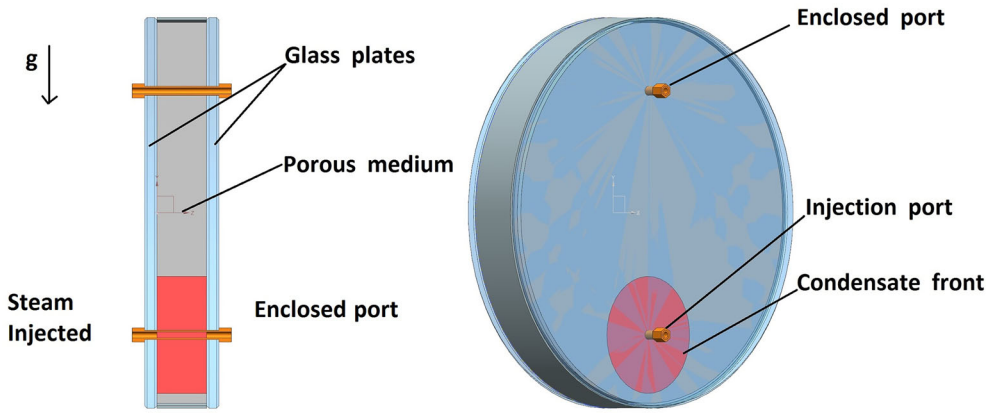

Fig. 7 Experimental array of the steam injection into the radial porous cell

Table 2 General parameters used in the experiments

Experiment	Injection pressure (kPa)	Flow rate (m^3/s)	Froude number (Fr)
4	49.1	$Q = 9.980\ E^{-7}$	$Fr = 0.0016$
5	245.1	$Q = 1.022\ E^{-5}$	$Fr = 0.1036$
6	14.7	$Q = 2.114\ E^{-7}$	$Fr = 4.42\times 10^{-5}$

color from deep blue (that represents room temperature) to yellow, which represents the highest temperature, the steam motion allows the heating of the porous matrix so a circular shape can be observed.

The fifth experiment shows the displacement of the condensate front at an initial steam pressure $P_i = 245.1$ kPa. The radial cell has attained an injection temperature during the steam injection of $T_i = 411.68$ K. Under such conditions, condensates are displaced radially due to the injection pressure within a homogeneous matrix, making a radial condensate profile that could only be seen with the reflex camera, since the time for the condensate front to reach the boundary is much faster than the diffusion time, as it can be observed in Fig. 11. It could not be recorded by the IFT camera.

For the last series of experiments, we compare qualitatively results that were obtained through a commercial simulator SMG STARS, see Yang and Gates (2009) and the experiments which were carried out by ourselves. In our experiment, steam was injected at $P_i = 14.7$ kPa. We found that gravity forces had to be taken into account. We could also see the effects of steam injection into the porous media near the point of injection. The comparison can be observed in Fig. 12.

5 Conclusions

In this work, thermographic and digital visualization techniques were used to show the evolution of the condensates fronts developed in two different kinds of configurations. Digital visualization allowed us to follow and visualize the resulting condensate fronts and estimate its speed. Meanwhile, the thermographic visualization technique permitted us to track the resulting thermal gradients due to the heat exchange between the porous medium and the steam.

In Sect. 3, the experiments of steam injection in cylindrical tubes exhibited different behaviors when the injection pressure was varied, in which the resulting advance of condensate fronts within the non-consolidate matrix showed different patterns that goes from noses to a fully developed flow within a porous medium (piston-like).

For the second series of experiments reported in Sect. 4, the geometry consisted of a radial porous cell. The shape adopted by the condensed steam depended strongly upon the injection pressure as a consequence of the area increase. For this specific case, the movement of steam or the condensates were mainly radial, depending on the pressure of the steam injection. Low pressures only allowed the steam to move radially. On the other hand, at high pressures, the condensates front moved radially and in front of the steam.

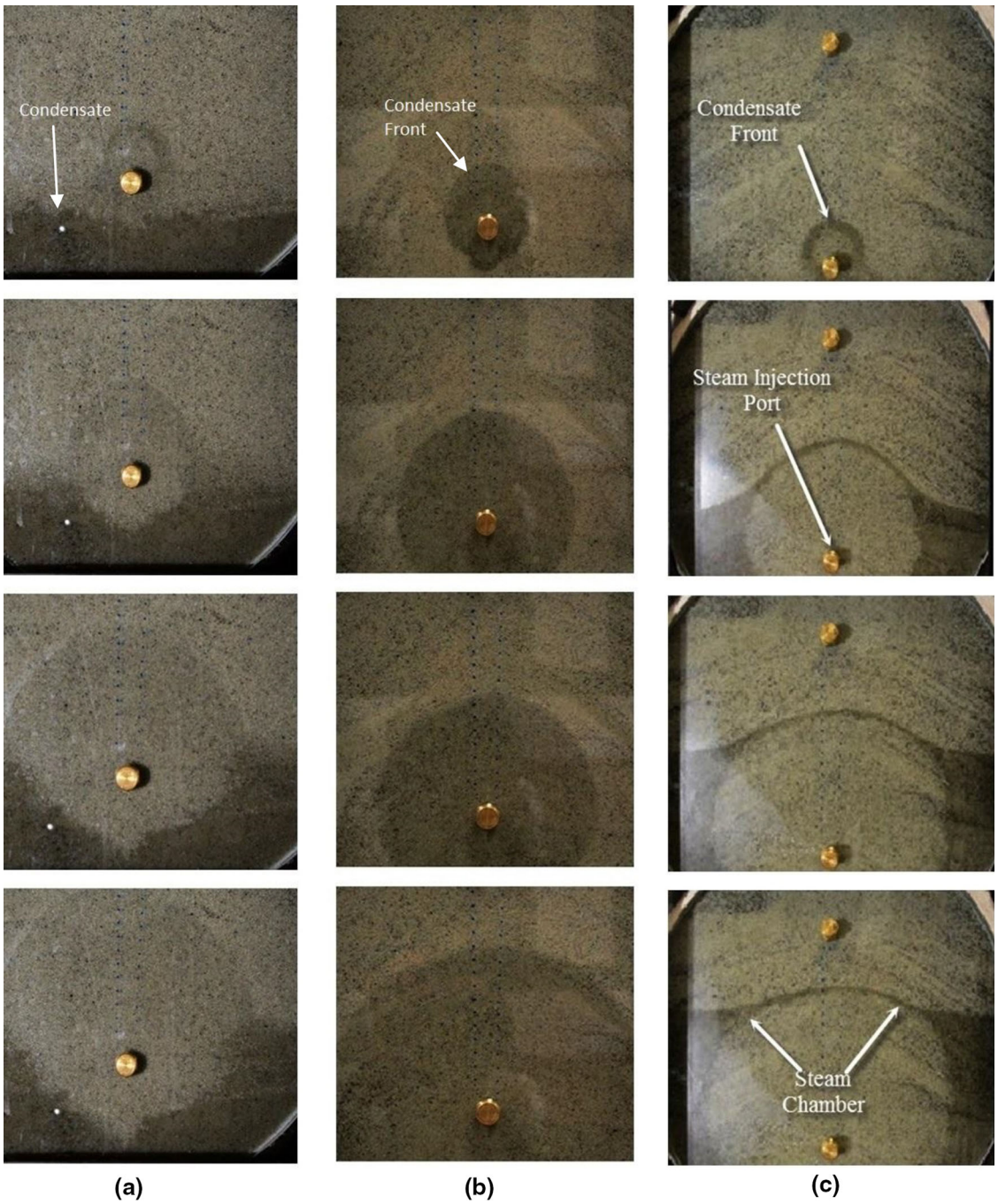

Fig. 8 Snapshots of the advance of the condensate front (*darker zones*) and steam front for (*clear zones* behind the *darker ones*) different injection pressures of **a** $P_i = 14.7$ KPa (*left-hand-column*), **b** $P_i = 49.1$ KPa (*middle-column*) and **c** $P_i = 245.1$ KPa (*right-hand-column*)

Since our purpose is to scale the laboratory results to an actual size oil field, some properties of the steam injection process will be discussed based on laboratory scale results and existing theoretical models. For the cylindrical tube that resembles the vertical injection of a fluid in a Geothermal reservoir, the gravity has influence on the motion of the condensates since it changes the shape of the front of condensate, as it was shown in Sect. 3.2. The shape of the condensate front was strongly influenced by the magnitude of the Froude Fr number. For the porous radial cell, that mimics the configuration of a real steam injection in a steam assisted gravity drainage (SAGD) process, gravity acts in a different manner. The magnitude of the

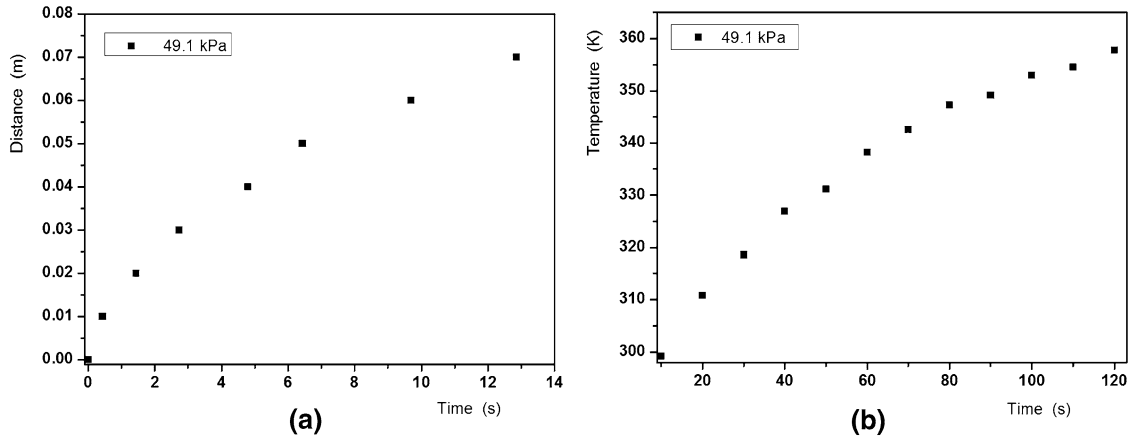

Fig. 9 Plots of the condensate front obtained for an injection pressure $P_i = 49.1$ kPa. **a** Plot of the displacement of the condensate front as a function of time. **b** Plot of the temperature profile as a function of time

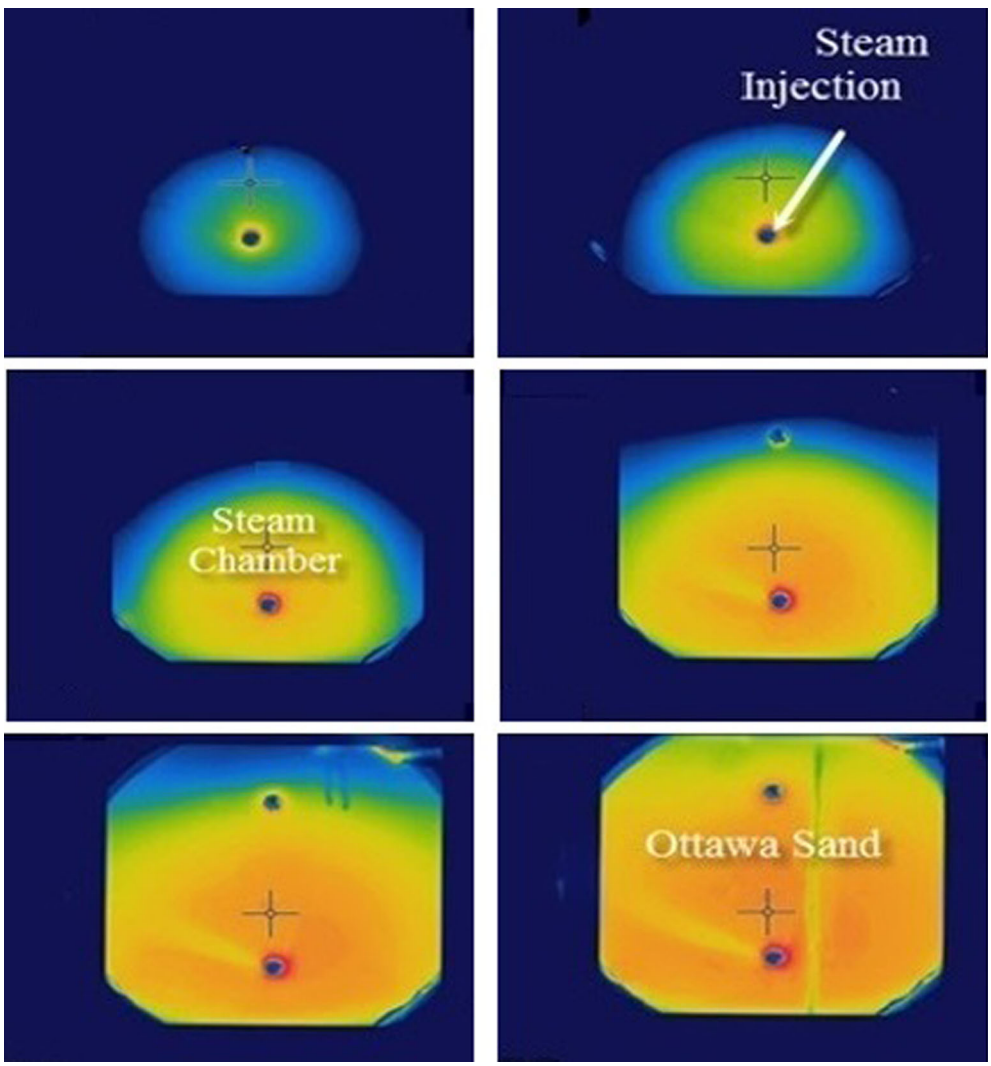

Fig. 10 Sequence of the IR pictures that show the evolution of the temperature distribution at an initial injection pressure of $P_i = 49.1$ kPa.

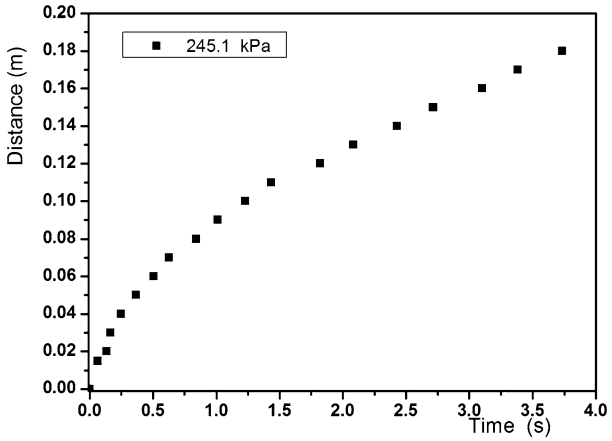

Fig. 11 Plot of the displacement of the condensate front as a function of time at $P_i = 245.1$ kPa

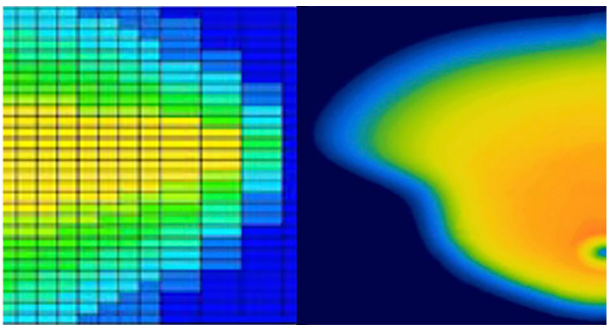

Fig. 12 Results obtained by Yang and Gates (2009) (*left*) vs. our results (*right*).

pressure, and the value of the Froude Fr number will tell us whether only one fluid moves radially, i.e.,, at low injection pressures the steam moves radially but the condensates only reach the bottom of the cell. At high pressures, both the steam and the condensates move radially, but the condensates advance at the front.

This study could be important for Geothermal and Petroleum applications, because it shows the behavior of steam in non-homogeneous porous medium with two critical arrangements. As we can see, the movement of the fluids into the reservoir can be taken from laboratory to operation scale and be optimized by estimating the value of the Froude Fr number.

Acknowledgments We would like to thank the SENER-CONACYT project "Integrated system for generating steam downhole" No. 147061 for supporting this study, SIP project "Submerged Jet of PIV No. 20151924, CONACYT for the scholarship "and the Laboratory of the Chemical Engineering and Extractive Industries (ESIQUE) IPN for allowing us to use their facilities.

References

Astarita T, Carlomagno GM (2013) Infrared thermography for thermo-fluid-dynamics. Springer, New York
Baskaya S, Gilchrist A, Fraser SM (1998) Mixing characteristics of turbulent water vapour jets measured using an isokinetic sampling probe. Exp Fluids 24:27
Butler RM, Yee CT (2002) Progress in the situ recovery of heavy oils and bitumen. J Can Pet Technol 41:31
Butler RM (1991) Thermal recovery of oil and bitumen. Prentice Hall, New Jersey
Castanie LM, Gadelle C (1991) Hot fluid injection Basic concepts in enhanced oil recovery processes. M Bavitre 33:271
Chung KH, Butler RM (1989) A theoretical and experimental study of steam-assisted gravity drainage process 4:191
Dudfield P, Woods A (2012) On the periodic injection of fluid into, and its extraction from, a porous medium for seasonal heat storage 707:467–481
Geertsma J, Croes GA, Schwarz N (1956) Theory of dimensionally scaled models of petroleum reservoirs. Trans AIME 207:118–127

Jabbour C, Quintard M, Bertin H, Robin M (1996) Oil recovery by steam injection: three-phase flow effects. J Pet Sci Eng 16:109
Leverett MC (1940) Capillary behavior in porous solids. Petroleum Technology, Petroleum Technology 152
Li K, Horne RN (2002) A scaling method for spontaneous imbibition in systems with different wettability, Proc. Intl. Symposium Soc. Core Analysts, stanford univesity, California 1–14
Nield DA, Bejan A (2006) Convection in porous media. Springer, New York
Rincón AC, Diaz-Muñoz J, Ali SMF (1970) Sweep efficiency in steamflooding. J Can Pet 175
Shreve DR, Welch LW, Krebill FK (1956) Gas drive and gravity drainage analysis for pressure maintenance operations, petroleum transactions. AIME 207:136
Tang Q, Gadelle F (2006) Heavy-oil solution gas drive in consolidated and unconsolidated rock. Soc Pet Eng SPE J 11:259
White DE, Muffler LJP, Truesdell AH (1974) Vapor-dominated hydrothermal systems compared with hot water systems 66:75
William BT, Valleroy VV, Rumberg GW, Cornellius AJ, Powers LW (1961) Laboratory studies of oil recovery by steam injection. Petroleum Technology 681
Woods AW (1999) Liquid and vapour flow in superheated rock. Ann Rev Fluid Mech 31:171
Woods AW, Fitzgerald SD (1993) The vaporization of a liquid front moving through a hot porous rock. J Fluid Mech 251:563
Yang X, Gates ID (2009) Design of hybrid steam-in situ combustion bitumen recovery processes. Nat Resour Res 18(3):213–233
Yortsos YC (1984) Distribution of fluid phases within the steam zone in steam-injection processes. Soc Pet Eng J 24(4):458–466
Yun TS, Santamarina JC (2008) Fundamental study of thermal conduction in dry soils. Granul Matter 10:197–207